

# Research Journal of Pharmaceutical, Biological and Chemical Sciences

## Electrochemical Behavior Of Pitting Corrosion Of X-60 Type Carbon Steel In Oil Wells Formation Water In The Absence And Presence Of Benzyldimethyldodecylammonium Bromide.

M. A. Migahed<sup>a</sup>, M.M. Attya<sup>b\*</sup>, S. M. Rashwan<sup>c</sup>, M. M. Kamel<sup>c</sup>, and A. M. Al-Sabagh<sup>a</sup>.

<sup>a</sup> Egyptian Petroleum Research Institute (EPRI), Nasr City, Cairo 11727, Egypt.

<sup>b</sup> Production engineering department, Badr Petroleum Company (BAPETCO), Heliopolis, Cairo, Egypt.

<sup>c</sup> Chemistry Department, Faculty of Science, Suez Canal University, Ismailia, Egypt.

### ABSTRACT

Chloride induced pitting corrosion of low carbon steel alloy in oil wells formation water was studied by anodic cyclic polarization. Pitting corrosion behavior was followed up by calculating pitting potential, re-passivation potential and anodic cyclic loop area. Pitting corrosion inhibition of benzyldimethyldodecylammonium bromide was evaluated in terms of protection against pitting nucleation and protection against pitting growth. Electrochemical impedance spectroscopy used to assess corrosion inhibition efficiency. Carbon steel surface and the nature of the formed protection film were investigated by using SEM and EDX measurements.

**Keywords:** Carbon steel, EIS, SEM, Pitting corrosion

*\*Corresponding author*

## INTRODUCTION

Carbon steel alloys are commonly employed for the construction of separators, pipelines, absorber towers, heat exchangers and reboilers of oil and gas treatment facilities [1]. Oil and gas production streams associate with formation water that may contain corrosive species such as chloride. Significant amounts of hydrogen sulfide, carbon dioxide and chloride lead to severe corrosion problems for oil and gas production assets [2-4]. The presence of chloride, bromide, thiocyanate and thiosulfate ions is the main cause of pitting corrosion. Chloride is considered the most aggressive species for inducing pitting corrosion [5, 6]. Pitting corrosion is considered to have extremely harmful impact on oil and gas production assets when compared to uniform corrosion type since formation of pits leads to external fluid leakage which have its relevant safety and environmental impacts and acquires equipment shutdown to overhaul the section where the pits formed. A lot of studies have been made on pitting behavior of variety of steel alloys [7-19].

Pitting corrosion is a localized attack where metal is removed preferentially from susceptible areas on the surface [20]. The process of localized corrosion is initiated by the breakdown of passive film on metal surface; then meta-stable growth of small pits on the verge of stability and finally stable growth of localized corrosion sites that can grow quite large [20]. Localized corrosion initiates above a critical potential known as pitting potential  $E_{pit}$  "breakdown potential of passivity" or "critical potential for pit nucleation" while repassivate below another lower potential known as repassivation potential  $E_{rp}$  [20]. Determination of both  $E_{pit}$  and  $E_{rp}$  permits quantitative evaluation of the resistance against pitting nucleation and resistance against pitting growth of a given metal under specific conditions.

The present work aims to study the pitting corrosion behavior of API 5L X 60 type carbon steel alloy in formation water containing chloride ion and evaluate the performance of a pre-synthesized cationic inhibitor as pitting corrosion inhibitor under such conditions. The corrosive media was prepared to resemble an actual operating process stream flowing through shell and tube heat exchanger in a gas treatment plant where the tube bundle of the heat exchanger suffers from severe pitting attack. Electrochemical techniques such as potentiodynamic polarization and electrochemical impedance spectroscopy were used to study the uniform corrosion while anodic cyclic polarization measurements, or in other words pitting corrosion technique, was used to study the pitting corrosion behavior. Finally, scanning electron microscopy (SEM) and energy dispersive X-ray (EDX) techniques were used to investigate the surface morphology of the investigated carbon steel alloy.

## EXPERIMENTAL

### Preparation of working electrode for electrochemical measurements

Table (1) shows the chemical composition of API 5L X 60 type carbon steel alloy employed in this work which was selected to resemble the material of construction of pipeline transporting oil well formation water to a treatment plant operating in western desert area in Egypt.

Table 1: Chemical composition of API 5L X 60 type carbon steel alloy

Element	C	Mn	Si	P	S	Al	Cr	Ni	V	Cu	Mo	Nb	Ti	Fe
Content (Wt %)	0.18	1.22	0.4	0.015	0.008	0.02	0.3	0.3	0.02	0.3	0.08	0.01	0.03	balance

Working electrode was made of the above mentioned carbon steel alloy in the form of cylindrical rod. The electrode was insulated with a strong adherent resin composite leaving an exposed area of  $1 \text{ cm}^2$ . Prior every electrochemical test, the working electrode was briefly abraded with emery papers up to grade 2000, then washed with bidistilled water and rinsed with acetone.

## Formation water

Table (2) shows the chemical composition of the corrosive media employed in this work. The chloride content is 21,120 ppm.

**Table 2: Chemical composition of formation water**

Ionic species	SO <sub>4</sub> <sup>2-</sup>	PO <sub>4</sub> <sup>3-</sup>	Cl <sup>-</sup>	Ca <sup>2+</sup>	Mg <sup>2-</sup>	Ba <sup>2+</sup>	K <sup>+</sup>	Zn <sup>+</sup>	T.D.S
Value (ppm)	6.5	0.771	21120	800	364	105	250	1.359	38520

## Specification of cationic inhibitor

Figure 1 shows the chemical structure of benzyldimethyldodecylammonium bromide. It was obtained from Sigma-Aldrich chemical supplier (product number B5776, CAS-No. 7281-04-1).

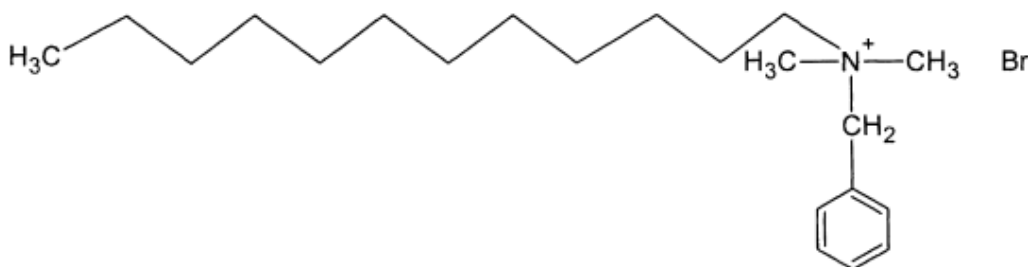


**Figure 1: Chemical structure of benzyldimethyldodecylammonium bromide.**

## Electrochemical measurements

Electrochemical experiments employed in this study were conducted in a 100 ml glass electrochemical cell using platinum wire as an auxiliary electrode and saturated calomel electrode (SCE) as a reference electrode. All tests were conducted at 25 °C using working electrode as specified in section 2.1. All potential values indicated in this work were measured against SCE reference electrode. The tip of reference electrode was placed close to the surface of the working electrode to minimize the IR drop. Electrochemical behavior of working electrode against corrosive media described in section 2.2 was studied.

## Open circuit potential measurement

Open circuit potential for working electrode was recorded over time for a period of 3 hours under formation water containing 21,120 ppm chloride ion at 25 °C with and without different concentrations of benzyldimethyldodecylammonium bromide. The test period was maintained to ensure achieving a stable potential value.

## Pitting corrosion test

Pitting corrosion test is an available pre-configured test in Volta master 4 software that controls Voltalab80 potentiostat apparatus. The test is an anodic cyclic polarization technique that allows user to specify a lot of test settings to control the anodic cyclic polarization loop. All experiments were initially polarized at -1000 mV with a scan rate of 2 mVs<sup>-1</sup>. Current threshold was determined at 2 mA/cm<sup>2</sup> at which the potential starts to reverse in the cathodic direction. The test is ended at either when potential reached -1000 mV again or the current decreases to 0 mA/cm<sup>2</sup>, i.e. which of them comes first.

### Electrochemical impedance spectroscopy

Electrochemical impedance measurements were carried out by applying a frequency range of 100 kHz to 20 mHz using 10 steps per frequency decade while 10 mV amplitude peak to peak AC signal was used to perturb the system. Voltalab80 apparatus was employed as described in section 2.4.2.

### Investigation of surface morphology

#### Energy dispersive analysis of x-rays (EDX)

Characterization of the adsorption film formed on the surface of the working electrode was examined using EDX system attached with a JEOL JSM-5410 scanning electron microscope. EDX spectra of abraded, blank and inhibited samples were compared to indicate the changes on carbon steel surface in the absence and presence of benzyldimethyldodecylammonium bromide.

#### Scanning electron microscopy (SEM)

The surface morphology of carbon steel surface was examined using scanning electron microscope (JEOL JSM-5410). The energy of the acceleration beam employed was 30 KV. All micrographs were taken at a magnification power ( $X = 100$ ).

#### Quantum chemical study

The molecular parameters were carried out based on MINDO3 semi-empirical method at a Unrestricted Hartree Fock (UHF) level which are implemented in Hyperchem 8.0. The molecules 2D sketch was obtained by ISIS Draw version 2.1.4 [21].

## RESULTS AND DISCUSSION

### Open circuit potential measurement

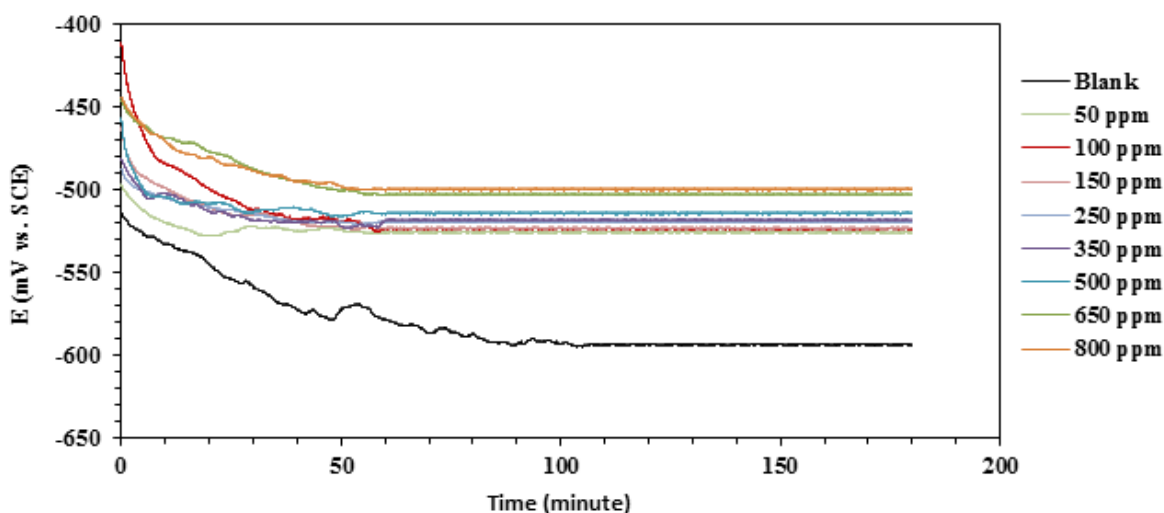


Figure 2: Open circuit potential versus time plots for X 60 type carbon steel alloy in the absence and presence of various concentrations of benzyldimethyldodecylammonium bromide at 25 oC.

Figure 2 shows the open circuit potential for the working electrode over time under formation water containing 21120 ppm chloride. The first moments of immersion time shows a rapid increase of open circuit potential towards more negative values. This indicates a high corrosion process at electrode surface. The rate of

such decrease in potential values tends to decrease gradually with time until reaching a steady state potential which corresponds to free corrosion potential. By increasing benzyldimethyldodecylammonium bromide concentration, OCP was shifted towards more noble direction. This indicates the anodic inhibition effect of the inhibitor and decrease the activity of electrochemical processes taken place at the electrode surface [22, 23]. Figure 2 also indicates that the time required for achieving the steady state potential is minimized after the addition of the inhibitor molecules with respect to blank. This minimization is also dependent on the concentration of cationic inhibitor which indicates a good surface coverage for the inhibited samples.

### Pitting corrosion test

Anodic cyclic polarization measurements were conducted for the working electrode in formation water containing 21120 ppm chloride at 25 °C. The potential scan rate was fixed for all experiments at 2 mVs<sup>-1</sup>. The current threshold at which the potential starts to reverse was maintained at 2 mA/cm<sup>2</sup>. Figure 3 shows a sample pitting corrosion test results. It can be noticed that by applying an anodic potential on the working electrode surface the passing current is minimal at this region which is the passive region. Then when the potential reaches a critical value, the current increased dramatically denoting the breakdown of passivity. This potential is called the break down potential of passivity or in other words pitting potential ( $E_{pit}$ ). The more positive the ( $E_{pit}$ ) is the more resistance against pitting nucleation. Beyond the ( $E_{pit}$ ) value, the nucleated pits start to grow up until the current reaches the predetermined threshold value, so that the potential will reverse. The reverse scan shows a wide hysteresis cyclic loop which is characteristic of passivity breakdown on the upward sweep and repassivation on the reverse sweep. The repassivation potential ( $E_{rp}$ ) is attained when the observed current returns to its minimal value again which corresponds to surface repassivation. The repassivation potential ( $E_{rp}$ ) represents the limit below which the metal remains passive and can be calculated as where the forward and reverse scan crosses. The smaller the hysteresis loop the easier it repassivate the nucleated pits.

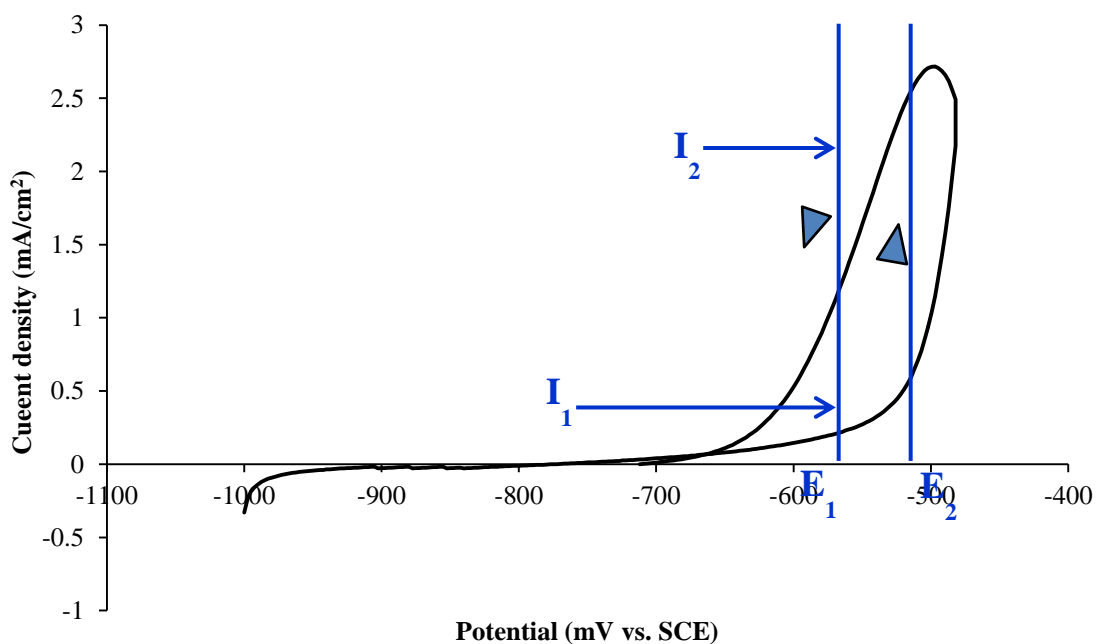


Figure 3: Representation of anodic cyclic polarization measurement (pitting corrosion test).

According to Figure 3, if we consider a potential value of  $E_1$  and draw a vertical line crossing the hysteresis loop at two different current values  $I_1$  and  $I_2$ . Even the potential value is the same, however it corresponds to two different corrosion current values. The smaller current value,  $I_1$ , corresponds to the initial propagation of pits which lies on the forward direction of the anodic cyclic loop. The higher current value,  $I_2$ , lies on the reverse

direction of the anodic cyclic hysteresis loop which indicates that the surface is hardly to passivate at this stage due to previously formed pits which was happened in the time between  $E_1$  and  $E_2$  values. As expected,  $I_2$  value is quite higher than  $I_1$  value in spite of having same applied potential value ( $E_1$ ). This can be attributed to the severe growth of the formed pits during polarizing the surface from  $E_1$  value to  $E_2$  value. The more the applied anodic potential the more pit growth is. Also, the applied potential scan rate impacts the hysteresis loop geometry. So that the scan rate is kept constant for all executed pitting corrosion tests to keep a valid comparison between the obtained results. It can be concluded that the narrower the hysteresis loop the closer  $I_1$  and  $I_2$  values of same applied potential, and hence the stronger inhibition efficiency of the applied inhibitor.

Figure 4 shows the measured pitting corrosion plot for uninhibited sample and 50 ppm inhibited sample. It is noted that both pitting potential ( $E_{pit}$ ) and repassivation potential ( $E_{rp}$ ) are shifted towards less negative values. This means that the working electrode surface in case of inhibited solution able to withstand more anodic potential prior having a significant increase in the measured current. i.e. its  $E_{pit}$  value shifted to the anodic direction. It is also noted that the hysteresis loop became narrower in case of the inhibited solution which demonstrates that the applied cationic inhibitor facilitate the repassivation potential, or in other words the electrode surface was passivated faster in case of inhibited solution.

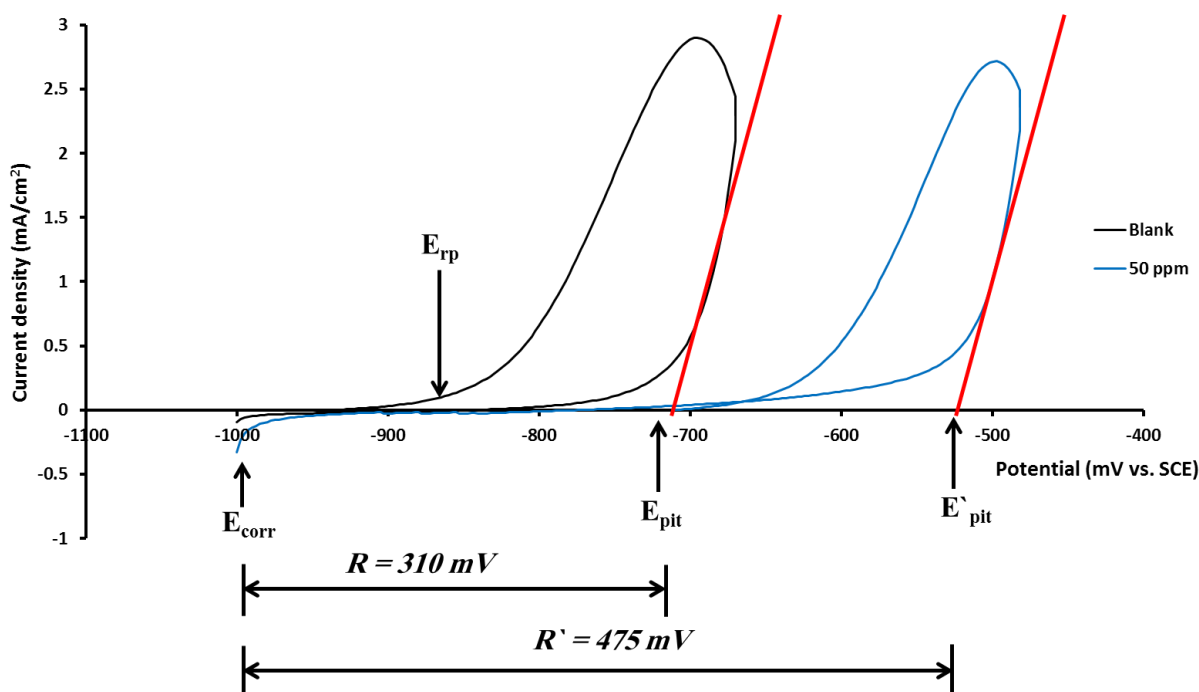


Figure 4: Schematic diagram showing the calculation of pitting potential ( $E_{pit}$ ), repassivation potential ( $E_{rp}$ ) and inhibition efficiency of pitting nucleation ( $P_{pit}$ ).

Pitting inhibition efficiency can be evaluated in terms of two important parameters. The first one is resistance against formation of new pits and the second one is the resistance against growth of old pits or pitting propagation. The first factor can be evaluated by calculating the shifting of pitting potential ( $E_{pit}$ ) with respect to the corrosion potential ( $E_{corr}$ ). The difference between  $E_{pit}$  and  $E_{corr}$  is referred here as  $R$  value which can be used as a comparative parameter to evaluate the resistance against pitting nucleation [20].  $P_{pit}$  is designated here as protection degree against pitting nucleation and calculated as percentage increase in the parameter  $R$  with respect to the reference value of  $R^0$  in the blank case.

The resistance of pitting propagation is evaluated in terms of the relative decrease of the area of the formed anodic hysteresis loop observed for each test run plotted in the form of potential against current density

as shown in Figure 5 [20]. The hysteresis loop area was calculated using an attached property of the analysis software Volta Master4.

$P_g$  is designated as protection against pitting growth and calculated as the percentage decrease of the hysteresis loop area with respect to the blank case. Figure 5 shows the anodic cyclic polarization plots for working electrode in the absence and presence of various concentrations of cationic inhibitor. It is noted that by increasing inhibitor concentration, both pitting potential  $E_{pit}$  and repassivation potential  $E_{rp}$  were shifted towards the anodic direction with narrower hysteresis loop area. This demonstrates that the applied cationic inhibitor resists the formation of new pits and also fasts repassivation of the working electrode moreover resists pitting growth.

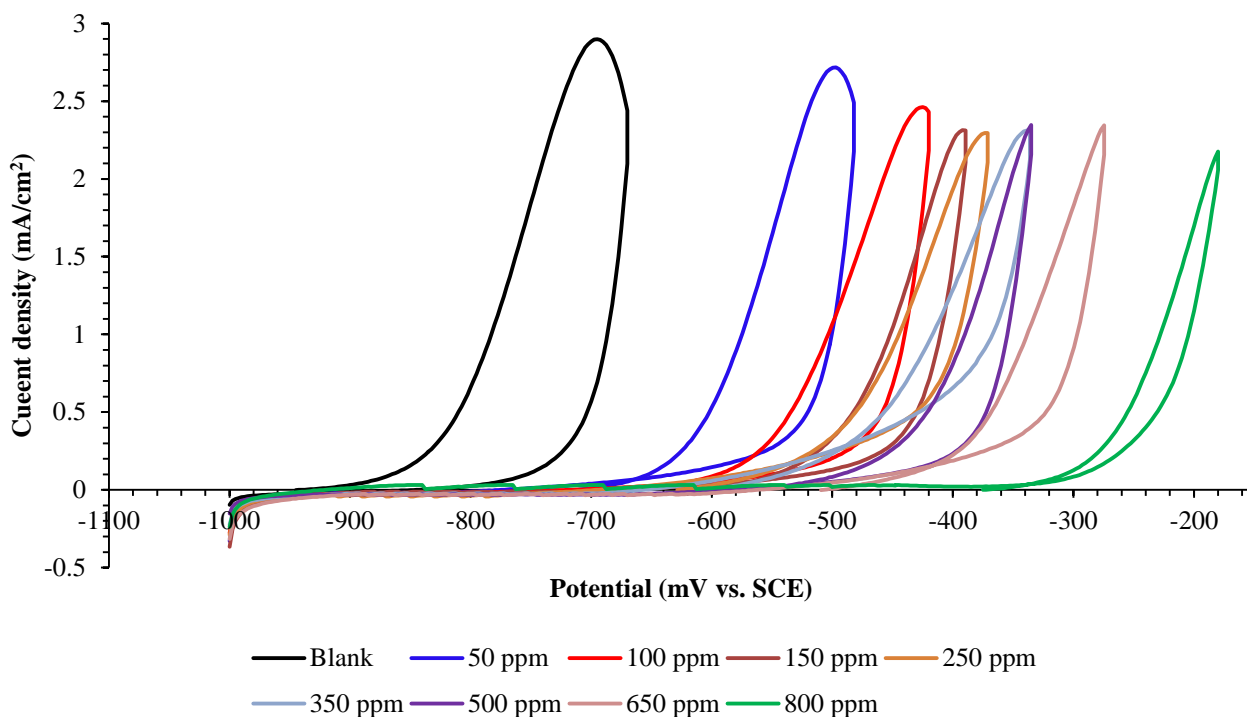


Figure 5: Pitting corrosion tests for X 60 type carbon steel alloy in the absence and presence of various concentrations of benzyltrimethyldecylammonium bromide at 25 °C.

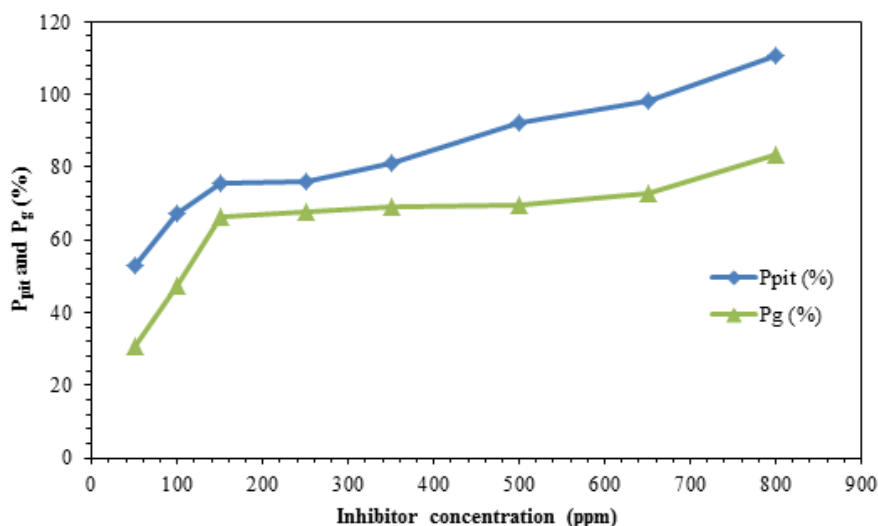


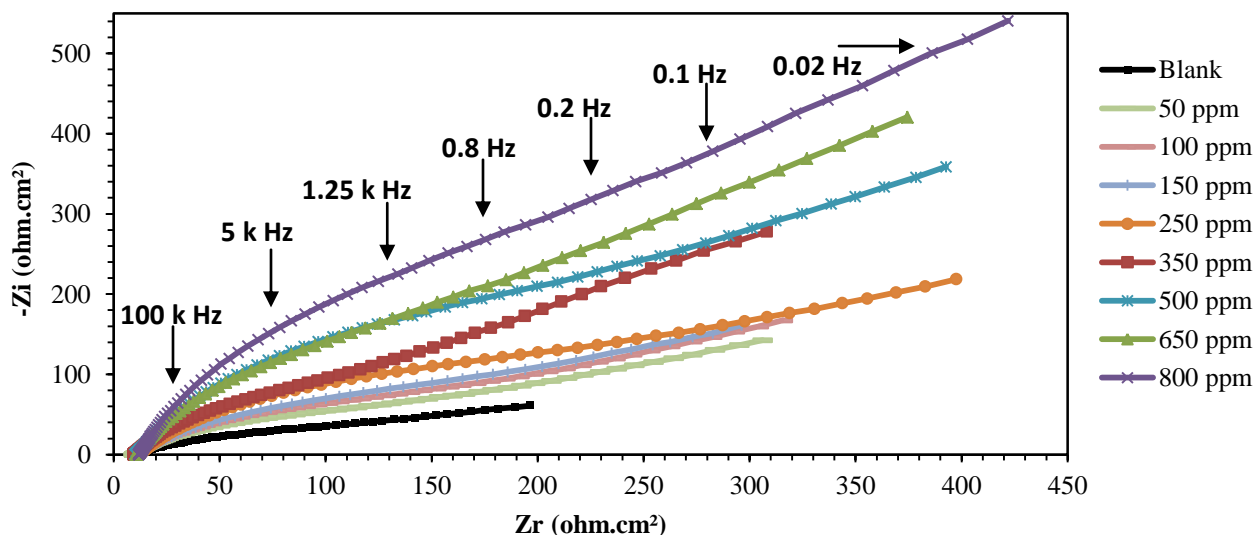
Figure 6: Performance of benzyltrimethyldecylammonium bromide against pitting nucleation ( $P_{pit}$ ) and pitting propagation ( $P_g$ ).

Table 3 summarizes the calculated pitting inhibition parameters of inhibited and uninhibited samples under testing conditions while Figure 6 plots resistance of pitting growth  $P_g$  and resistance of pitting nucleation  $P_{pit}$  against inhibitor concentration. It is worthy to mention that both the calculated  $P_{pit}$  and  $P_g$  values can go beyond 100% since it were used as a comparative values not as absolute values.

**Table 3: Pitting corrosion test parameters obtained for X-60 carbon steel in formation water containing various concentrations of benzyldimethyldodecylammonium bromide**

Conc.	$E_{rp}$ (mV vs. SCE)	$E_{cor}$ (mV vs. SCE)	$E_{pit}$ (mV vs. SCE)	R (mV)	$P_{pit}$ (%)	$P_g$ (%)
Blank	-840	-1020.6	-710	311	-	-
50 ppm	-632	-1006.8	-532	475	52.89	30.62
100 ppm	-565	-990.3	-471	519	67.09	47.19
150 ppm	-522	-982.4	-437	545	75.45	66.20
250 ppm	-521	-967.7	-421	546	76.02	67.56
350 ppm	-501	-952.6	-391	562	80.94	69.16
500 ppm	-435	-972.1	-375	597	92.29	69.75
650 ppm	-412	-948.3	-332	616	98.36	72.96
800 ppm	-290	-894.7	-240	654	110.71	83.52

**Electrochemical impedance spectroscopy**



**Figure 7: Nyquist plots for X 60 type carbon steel alloy in the absence and presence of various concentrations of benzyldimethyldodecylammonium bromide at 25 °C.**

Figure 7 shows Nyquist impedance plots for X 60 type carbon steel alloy in the absence and presence of various concentrations of cationic inhibitor at 25 °C. It is noticed that the impedance curves were changed after the addition of cationic inhibitor molecules. The obtained impedance spectra was modeled using Boukamp

software to construct the equivalent circuit (EC) as shown in Figure 8 where  $R_s$  is the solution resistance,  $R_t$  is the charge transfer resistance,  $C_{dl}$  is the electrochemical double layer capacitance,  $R_f$  represents the film resistance and  $C_f$  represents the film capacitance.

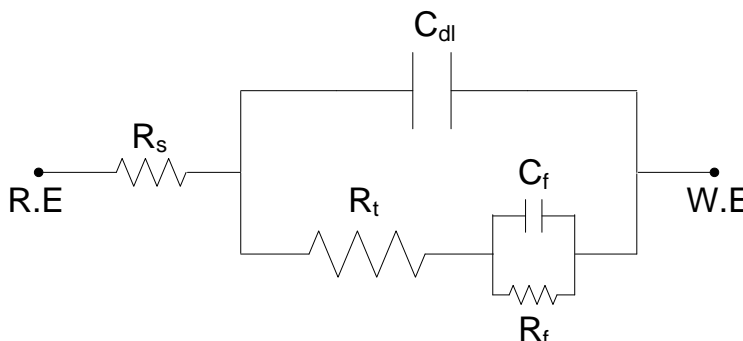


**Figure 8: Equivalent circuit used to model impedance measurements calculated for X 60 type carbon steel alloy in the absence and presence of various concentrations of benzyldimethyldodecylammonium bromide at 25 °C.**

The equivalent circuit was used for the interpretation of impedance spectra upon which both charge transfer resistance  $R_t$  and adsorption film resistance  $R_f$  were calculated. Electrochemical double layer capacitance  $C_{dl}$  was obtained at the frequency  $f_{max}$ , at which the imaginary component of the impedance is maximal –  $Z_{max}$  using the following equation [24]:

$$C_{dl} = \frac{1}{2\pi f_{max}} \frac{1}{R_t} \quad (1)$$

Finally, the percentage inhibition efficiency IE % was calculated from the values of  $R_t$  using the following equation:

$$IE\% = \left(1 - \frac{R_t}{R_{t(inh)}}\right) \times 100 \quad (2)$$

where  $R_t$  and  $R_{t(inh)}$  are the charge transfer resistance values in the absence and presence of inhibitor, respectively. Table 4 summarizes the obtained EIS parameters and the calculated percentage inhibition efficiency IE%. A good fitting of equivalent circuit is indicated by the high coefficient values as shown in Table 4.

**Table 4: Data obtained from electrochemical impedance spectroscopy (EIS) measurements of X 60 type carbon steel alloy in the absence and presence of various concentrations of benzyldimethyldodecylammonium bromide at 25 °C.**

Conc.	Coeff.	$R_s$ (ohm.cm <sup>2</sup> )	$R_f$ (ohm.cm <sup>2</sup> )	$C_f$ (μF/cm <sup>2</sup> )	$R_t$ (ohm.cm <sup>2</sup> )	$C_{dl}$ (μF/cm <sup>2</sup> )	IE%
Blank	0.988	9.099	-	-	167.72	7589	-
50 ppm	0.956	10.24	12.43	74.53	357.8	5018	53.12
100 ppm	0.959	10.06	16.53	68.32	499.9	4750	66.45
150 ppm	0.982	10.89	21.58	62.72	539.2	4533	68.89
250 ppm	0.977	11.01	27.53	50.34	712.2	4031	76.45
350 ppm	0.97	10.73	32.26	43.86	750	3996	77.64
500 ppm	0.981	9.12	36.74	38.12	796	3354	78.94
650 ppm	0.985	9.83	39.43	27.56	1114	3141	84.95
800 ppm	0.987	10.62	41.37	22.05	3048	3131	94.50



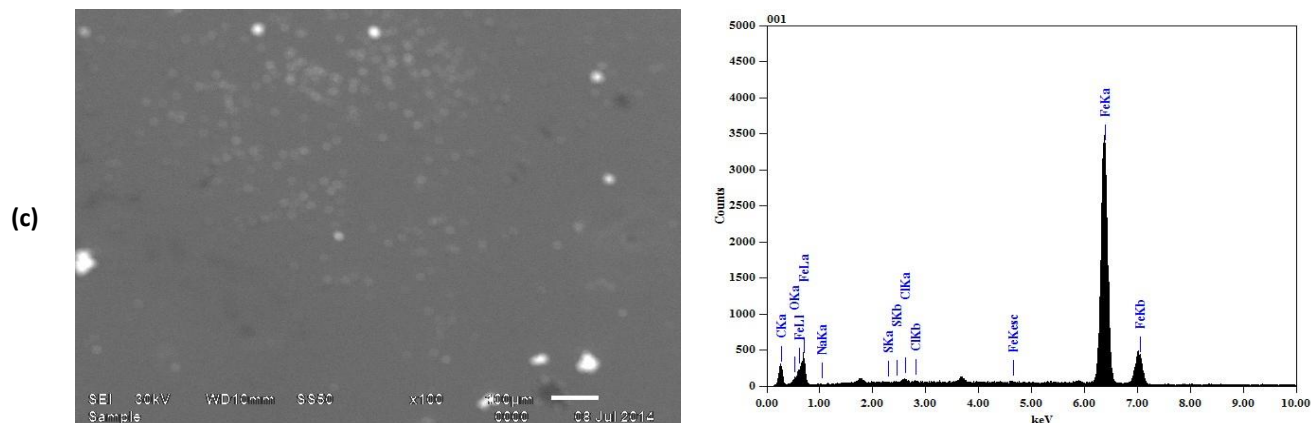


**Figure 9: SEM and EDX spectra of carbon steel surface: (a) polished sample, (b) after immersion in oil well formation water and (c) after immersion in oil well formation water in the presence of 800 ppm of benzyldimethyldodecylammonium bromide.**

### Quantum chemical study results

Quantum chemical studies have been successfully implemented to verify the inhibition efficiency of organic inhibitor with their calculated molecular orbital (MO) energy level [28].

Quantum chemical parameters, which are thought important to directly influence on electronic interaction between iron surface and inhibitor, are listed in Table 5 namely the energy of the highest occupied molecular orbital ( $E_{\text{HOMO}}$ ), energy of the lowest unoccupied molecular orbital ( $E_{\text{LUMO}}$ ), the energy gap ( $\Delta E$ ), dipole moment ( $\mu$ ), the number of transferred electrons ( $\Delta N$ ), and the optimized geometry structures of the compounds were in Figure 10.

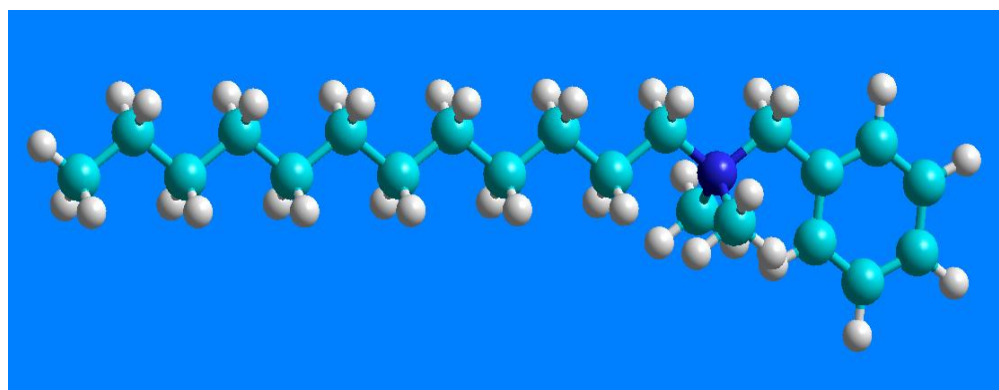


**Figure 10: Equilibrium structure of the inhibitor.**

**Table 5: Quantum chemical parameters of the investigated benzyldimethyldodecylammonium bromide.**

$E_{\text{HOMO}}(\text{eV})$	$E_{\text{LUMO}}(\text{eV})$	$\Delta E(\text{eV})$	$\mu(\text{debye})$	$\Delta N(\text{eV})$
-2.55	-0.77	1.78	0.115	-3.0

The inhibiting effect of this compound was attributed to their parallel adsorption at the metal surface by active centers for adsorption. Due to the planar geometry of the inhibitor, the molecular adsorption probably occurs in such a way that the metal surface and the molecular plane are parallel to each other by donation and back donation between the molecule and the metal surface. The planer geometry is clear in Figure 10. From Figure

10, these molecules have approximately planar structure, which can offer the largest contact area between the inhibitor molecules and the steel surface.

Frontier orbital theory is useful in predicting adsorption centers of the inhibitor molecules responsible for the interaction with surface metal atoms [29, 30]. Terms involving the frontier MO could provide dominative contribution, because of the inverse dependence of stabilization energy on orbital energy difference [31]. It has been reported in the literature that the higher the HOMO energy of the inhibitor, the greater the trend of offering electrons to unoccupied d orbital of the metal, and the higher the corrosion inhibition efficiency.

In addition, the lower the LUMO energy, the easier the acceptance of electrons from metal surface, as the LUMO–HOMO energy gap decreased and the efficiency of inhibitor improved [32]. The frontier molecule orbital density distributions for inhibitor are shown in Figure 11 (a-b). Quantum chemical parameters listed in Table 5 reveal that this inhibitor has high HOMO and low LUMO with high energy gap. The number of transferred electrons ( $\Delta N$ ) was also calculated according to the following equation [33, 34]

$$\Delta N = \frac{X_{Fe} - X_{inh}}{2(\eta_{Fe} - \eta_{inh})} \quad (3)$$

where  $X_{Fe}$  and  $X_{inh}$  denote the absolute electronegativity of iron and the inhibitor molecule, respectively;  $\eta_{Fe}$  and  $\eta_{inh}$  denote the absolute hardness of iron and the inhibitor molecule, respectively. These quantities are related to electron affinity (A) and ionization potential

$$X = (I + A)/2 \quad , \quad \eta = (I - A)/2 \quad (4)$$

I and A are related in turn to  $E_{HOMO}$  and  $E_{LUMO}$

$$I = -E_{HOMO} \quad , \quad A = -E_{LUMO} \quad (5)$$

Values of X and  $\eta$  were calculated by using the values of I and A obtained from quantum chemical calculation. The theoretical values of  $X_{Fe}$  and  $\eta_{Fe}$  are 7 and 0 eV/mol, respectively [33]. The fraction of electrons transferred from inhibitor to the iron molecule ( $\Delta N$ ) was calculated. According to other reports [33, 34], value of  $\Delta N$  showed inhibition effect resulted from electrons donation.

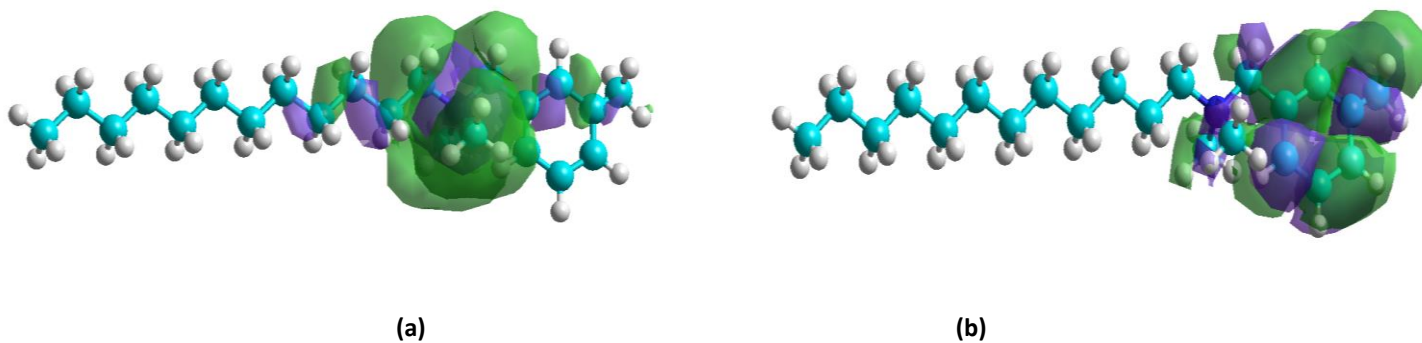


**Figure 11: The frontier molecule orbital density distributions of Inhibitor (a) HOMO and (b) LUMO**

The dipole moment ( $\mu$ ) is an index that can also be used for the prediction of the direction of a corrosion inhibition process [35]. Low values of the dipole moment will favor the accumulation of inhibitor molecules on the metallic surface.

### Molecular electrostatic potential

The molecular electrostatic potential (MEP) is related to the electronic density and is a very useful descriptor for determining sites for electrophilic attack and nucleophilic reactions as well as hydrogen-bonding interactions [36–38]. The electrostatic potential  $V(r)$  is also well suited for analyzing processes based on the recognition of one molecule by another, because it is through their potentials that the two species first "see" each other [39, 40]. As a real physical property,  $V(r)$  can be determined experimentally by diffraction or by computational methods [41].

To predict reactive sites for electrophilic and nucleophilic attacks for the title molecule. The negative red regions of MEP were related to electrophilic reactivity and the positive green regions to nucleophilic reactivity as shown in Figure 12. As can be seen from the figure, there is a possible site on the title compound for electrophilic attack. The negative region is localized on the nitrogen atom, with a maximum value of -0.3 a.u and carbon of benzene ring coming from the  $p_z$  orbital of  $\pi$  bond -0.03 a.u.

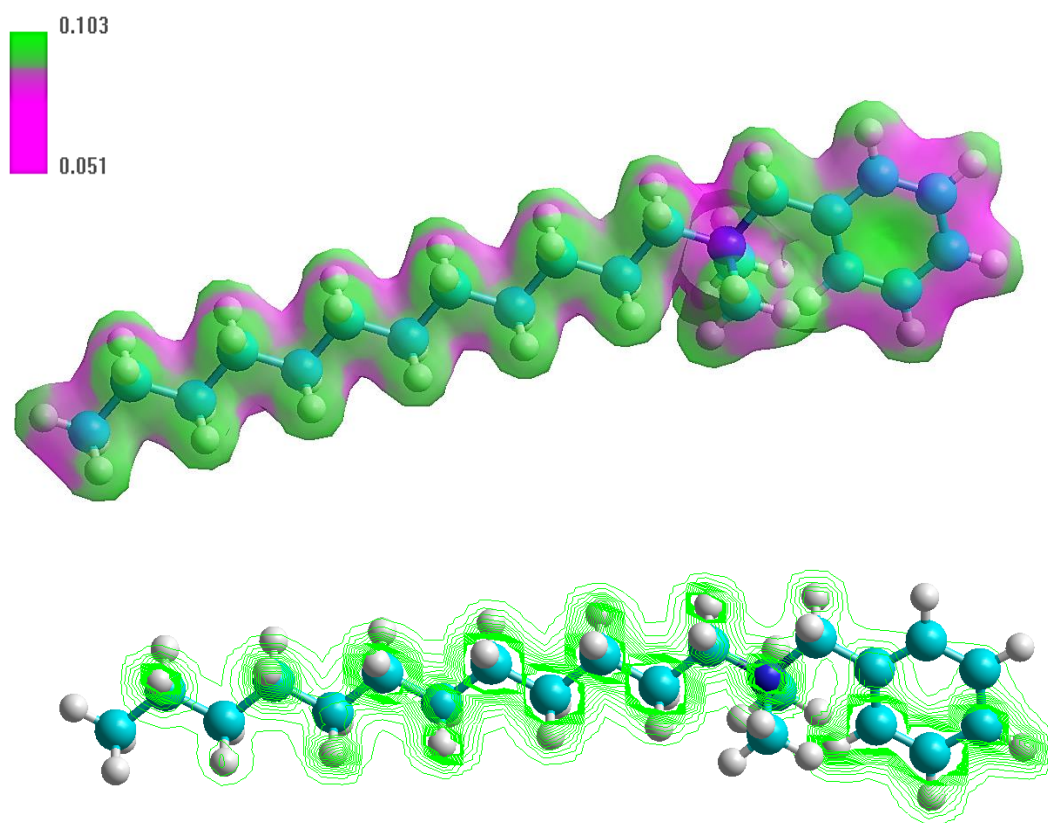


**Figure 12: Molecular electrostatic potential map of benzyldimethyldodecylammonium bromide.**

However, a maximum positive region is localized on dodecyl probably due to the hydrogen, with a maximum value of 0.038 a.u. This result provides information concerning the region where the compound can interact intermolecularly and bond covalently.

The Mulliken charge distribution of inhibitor is presented in Table 6. It could be readily observed that nitrogen atoms and the some carbons atoms of benzene ring had higher charge densities. The regions of highest electron density are generally the sites to which electrophiles attacked. Therefore N, and C atoms were the active center, which had the strongest ability of bonding to the metal surface. On the other hand, HOMO (Fig. 11a) was

mainly distributed on the area containing Nitrogen atom. Thus, the area containing nitrogen atom was probably the primary site of the bonding.

**Table 6: The charge density of some atom in benzyldimethyldodecylammonium bromide.**

No.	Atom	Charge
1	N	-0.321
2	C	-0.038
3	C	-0.031
4	C	-0.023
5	C	0.038

### CONCLUSION

- Benzyldimethyldodecylammonium bromide acts as a good pitting corrosion inhibitor for API X 60 carbon steel in oil well formation water containing chloride.
- The results of open circuit potential measurements revealed that OCP was shifted towards more anodic values by increasing inhibitor molecules.
- The presence of benzyldimethyldodecylammonium bromide molecules shortened the time required to establish the steady state potential (OCP).
- Anodic cyclic polarization measurements showed that pitting potential ( $E_{pit}$ ) was shifted towards more anodic values after applying cationic inhibitor under investigation.
- Re-passivation of carbon steel surface was faster in the presence of benzyldimethyldodecylammonium bromide with respect to blank sample.
- Addition of cationic inhibitor namely benzyldimethyldodecylammonium bromide increase protection against pitting nucleation and pitting growth.
- EIS technique confirmed formation of good protective film of inhibitor molecules on carbon steel surface.
- SEM images confirmed the obtained data from pitting corrosion test and electrochemical impedance spectroscopy.

### ACKNOWLEDGEMENT

The authors would like to express their appreciation for Egyptian Petroleum Research Institute (EPRI) for the financial support of this work.

### REFERENCES

- [1] D.A. Lopez, S.N. Simison, S.R. de Sanchez, The influence of steel microstructure on CO<sub>2</sub> corrosion. EIS studies on the inhibition efficiency of benzimidazole, *Electrochim. Acta* 48 (2003) 845-854.
- [2] D.B. Lebsack, D. Hawn, Internal pipeline rehabilitation using polyamide liners, *Mater. Perform.* 37 (1998) 24-27.
- [3] A.A. Gonik, Nature of abnormally-high corrosion of electric immersion pumps uetsn in development wells of oil deposits at the late stage of their development, *Zashchita Metallov* 32 (1996) 622-625.
- [4] Y.J. Tan, S. Bailey, B. Kinsella, A. Lowe, Mapping corrosion kinetics using the wire beam electrode in conjunction with electrochemical noise resistance measurements, *J. Electrochem. Soc.* 147 (2000) 530-539.

- [5] K. Aramaki, T. Shimura, Complete protection of a passive film on iron from breakdown in a borate buffer containing 0.1 M of  $\text{Cl}^-$  by coverage with an ultrathin film of two-dimensional polymer, *Corros. Sci.* 48 (2006) 209-225.
- [6] F.M. AL-Kharafi, B.G. Atea, R.M. AbdAlla, Electrochemical behaviour of low carbon steel in concentrated carbonate chloride brines, *J. Appl. Electrochem.* 32 (2002) 1363-1370.
- [7] *IJE Transactions B: Applications*, Vol. 22, No. 4, December 2009 (369-380)
- [8] S. Nagarajan, M. Karthega and N. Rajendran, Pitting corrosion studies of super austenitic stainless steels in natural sea water using dynamic electrochemical impedance spectroscopy, *J. Appl. Electrochem.* 37 (2007) 195-201
- [9] X. Jiang, Y.G. Zheng, D.R. Qu, W. Ke, Effect of calcium ions on pitting corrosion and inhibition performance in  $\text{CO}_2$  corrosion of N80 steel, *Corros. Sci.* 48 (2006) 3091-3108
- [10] Bo Deng, Yiming Jiang, Jiaying Liao, Yunwei Hao, Cheng Zhong, Jin Li, Dependence of critical pitting temperature on the concentration of sulphate ion in chloride-containing solutions, *Appl. Surf. Sci.* 253 (2007) 7369-7375
- [11] J.L. Polo, E. Cano, J.M. Bastidas, An impedance study on the influence of molybdenum in stainless steel pitting corrosion, *J. Electroanal. Chem.* 537 (2002) 183-187
- [12] P. Ernst, R.C. Newman, Explanation of the effect of high chloride concentration on the critical pitting temperature of stainless steel, *Corros. Sci.* 49 (2007) 3705-3715
- [13] Matjaž Finšgar, Stefan Fassbender, Sabine Hirth, Ingrid Milošev, Electrochemical and XPS study of polyethyleneimines of different molecular sizes as corrosion inhibitors for AISI 430 stainless steel in near-neutral chloride media, *Mat. Chem. Phys.* 116 (2009) 198-206
- [14] Yusuke Tsutsumi, Atsushi Nishikata, Tooru Tsuru, Pitting corrosion mechanism of Type 304 stainless steel under a droplet of chloride solutions, *Corros. Sci.* 49 (2007) 1394-1407
- [15] S.A.M. Refaey, F. Taha, A.M. Abd El-Malak, Inhibition of stainless steel pitting corrosion in acidic medium by 2-mercaptobenzoxazole, *Appl. Surf. Sci.* 236 (2004) 175-185
- [16] H. A. El Dahan, Pitting corrosion inhibition of 316 stainless steel in phosphoric acid-chloride solutions Part I Potentiodynamic and potentiostatic polarization studies, *J. Mat. Sci.* 34 (1999) 851-857
- [17] W. S. Li and J. L. Luo, Electrochemical investigations on formation and pitting susceptibility of passive films on iron and iron-based alloys, *Int. J. Electrochem. Sci.* 2 (2007) 627 - 665
- [18] L. Peguet, B. Malki, B. Baroux, Influence of cold working on the pitting corrosion resistance of stainless steels, *Corros. Sci.* 49 (2007) 1933-1948
- [19] T.L. Sudesh L. Wijesinghe, Daniel John Blackwood, Real time pit initiation studies on stainless steels: The effect of sulphide inclusions, *Corros. Sci.* 49 (2007) 1755-1764
- [20] S. Szklarska-Smialowska, *Pitting Corrosion of Metals*, D. 296, NACE, Houston, TX, 1986.
- [21] K.F. Khaled, The inhibition of benzimidazole derivatives on corrosion of iron in 1 M HCl solutions, *Electrochim. Acta* 48 (2003) 2493-2503.
- [22] K.M. Ismail, Evaluation of cysteine as environmentally friendly corrosion inhibitor for copper in neutral and acidic chloride solutions, *Electrochim. Acta* 52 (2007) 7811-7819.
- [23] J.R. Vilche, A.J. Arvia, Kinetics and mechanism of the nickel electrode-I. Acid solutions containing a high concentration of chloride and nickel ions, *Corros. Sci.* 15 (1975) 419-431.
- [24] A. P.; Yadav, A. Nishikata; Tsuru T.; Electrochemical impedance study on galvanized steel corrosion under cyclic wet-dry conditions-influence of time of wetness, *Corros. Sci.* 46 (2004) 169-181.
- [25] K.F.Khaled; Experimental and theoretical study for corrosion inhibition of mild steel in hydrochloric acid solution by some new hydrazine carbodithioic acid derivatives, *Appl. Surf. Sci.* 252 (2006) 4120-4128.
- [26] M.A. Migahed, M.A. Hegazy, A.M. Al-Sabagh, Synergistic inhibition effect between  $\text{Cu}^{2+}$  and cationic gemini surfactant on the corrosion of down hole tubing steel during secondary oil recovery of old wells, *Corros. Sci.* 61 (2012) 10 -18
- [27] ASTM E 45-87, vol. 11, ASTM, Philadelphia, PA, (1980) 125.
- [28] M. J. Bahrami, S.M. A. Hosseini, P. Pilvar, Experimental and theoretical investigation of organic compounds as inhibitors for mild steel corrosion in sulfuric acid medium, *Corros. Sci.* 52 (2010) 2793-2803
- [29] J. Fang, J. Li, Quantum chemistry study on the relationship between molecular structure and corrosion inhibition efficiency of amides, *J. Mol. Struct. (THEOCHEM)* 593 (2002) 179-185.

- [30] G. Bereket, E. Hur, C. Ogretir, Quantum chemical studies on some imidazole derivatives as corrosion inhibitors for iron in acidic medium, *J. Mol. Struct. (THEOCHEM)* 578 (2002) 79-88.
- [31] A.Y. Musa, A.A.H. Kadhum, A.B. Mohamad, M.S. Takriff, A.R. Daud, S.K. Kamarudin, On the inhibition of mild steel corrosion by 4-amino-5-phenyl-4H-1, 2, 4-triazole-3-thiol, *Corros. Sci.* 52 (2010) 526-533.
- [32] K.F. Khaled, Adsorption and inhibitive properties of a new synthesized guanidine derivative on corrosion of copper in 0.5 M H<sub>2</sub>SO<sub>4</sub>, *Appl. Surf. Sci.* 255 (2008) 1811-1818.
- [33] H. Ju, Z. Kai, Y. Li, Aminic nitrogen-bearing polydentate Schiff base compounds as corrosion inhibitors for iron in acidic media: A quantum chemical calculation, *Corros. Sci.* 50 (2008) 865-871.
- [34] I. Lukovits, E. Kalman, F. Zucchi, Corrosion inhibitors-correlation between electronic structure and efficiency, *Corrosion (NACE)* 57 (2001) 3-8.
- [35] Hansch, C.; Leo, A. *Substituentz for Correlation Analysis in Chemistry and Biology*; Wiley: New York, NY, USA, 1979.
- [36] E. Scrocco, J. Tomasi, Electronic molecular structure, Reactivity and intermolecular forces: An Euristic interpretation by means of electrostatic molecular potentials, *Adv. Quant. Chem.* 11 (1978) 115-193.
- [37] Luque, F. J., Lopez, J. M., & Orozco, M. (2000). *Theor. Chem. Accounts*, 103, 343.
- [38] N. Okulik, A. H. Jubert, Theoretical Analysis of the Reactive Sites of Non-steroidal Anti-inflammatory Drugs, *Internet Electron. J. Mol. Des.* 4 (2005) 17-30.
- [39] Politzer, P., Laurence, P. R., & Jayasuriya, K. (1985). *Environ. Health Perspect.* [Special issue], 61, 191.
- [40] Scrocco, E., & Tomasi, J. (1973). *Topics in Current Chemistry*, Springer: Berlin.
- [41] Politzer, P., & Truhlar, D. G. (1981). *Chemical Applications of Atomic and Molecular Electrostatic Potentials*, Plenum: New York.